# THE DESIGN AND CONSTRUCTION OF AN X-RAY DIFFRACTOMETER

By

Andrew C. Evans

A thesis submitted in partial fulfillment of the
requirements for the degree of

Bachelor of Science

Houghton College

October 2013

Signature of Author……..…….…….
Department of Physics
October 22, 2013

……..
Dr. Brandon Hoffman
Assistant Professor of Physics
Research Supervisor

……..
Dr. Mark Yuly
Professor of Physics

**THE DESIGN AND CONSTRUCTION OF AN X-RAY DIFFRACTOMETER**

By

Andrew C. Evans

Submitted to the Department of Physics
on October 22, 2013 in partial fulfillment of the
requirement for the degree of
Bachelor of Science

**Abstract**

X-ray diffractometry is an essential technique in the study of microscopic crystals and thin films. A Bragg-Brentano x-ray diffractometer has been designed and is currently under construction to be used in the Houghton College thin-film research lab. The diffractometer will be essential in studying the atomic lattice transitions and any high concentration impurities produced in silver thin films produced at this lab.

Thesis Supervisor: Dr. Brandon Hoffman
Title: Assistant Professor of Physics

TABLE OF CONTENTS

TABLE OF FIGURES

*Chapter 1*

# INTRODUCTION

## 1.1 The Discovery of X-rays

X-rays were an unobserved phenomenon until the development of high voltage vacuum tubes [1]. Crookes tubes, one of the types of high voltage vacuum tubes, were built to research the properties of streams of charge, which was necessary in the discovery and characterization of electrons [2]. It was these tubes that Wilhelm Röntgen used to discover x-rays. Röntgen placed a Crookes tube in a dark room and covered it so that no light emanating from it could be seen. In Figure 1 a diagram of a basic high voltage vacuum tube is shown with a cathode on the left side which emits the electrons. Röntgen discovered that a fluorescent screen would light up in proximity to the tube in the dark room. He coined the term 'x-ray' for this phenomenon as they were an unknown source of what was thought to be light radiation which induced fluorescence but did not seem to interact much with matter [1]. X-rays were created in the tube when the accelerated electron would strike either the anode or one of the glass sides of the tube. The sudden acceleration of electrons striking the glass or anode caused the emission of what was termed Bremsstrahlung radiation.

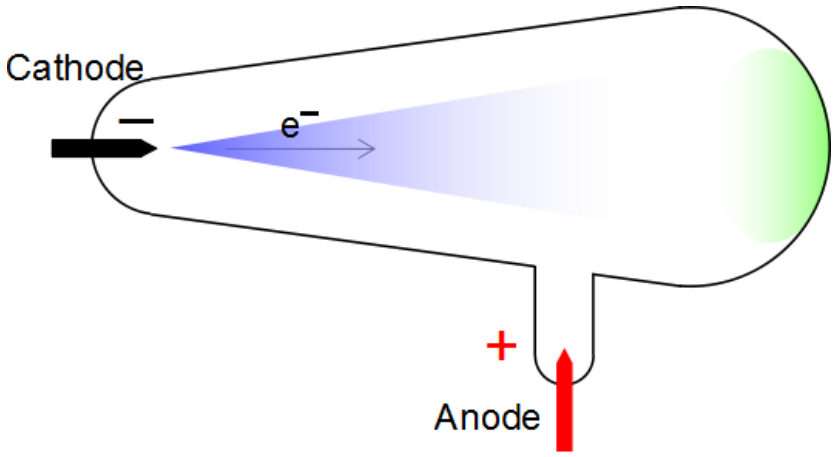


Figure 1. Diagram of a high voltage vacuum tube. Elecrons are emitted from the cathode on the left. The glow, colored blue, in the tube is caused by the gas ionized gas inside. The green glow is caused by electrons overshooting the anode and striking the glass wall.

In addition to creating x-rays through the process of bremsstrahlung, x-ray fluorescence was observed. The combination of these effects led to a distinct anisotropy in the x-ray radiation [1]. At certain electron energies, the tube would begin to 'glow' with x-rays. The incoming electrons would excite electrons in the target, which would then de-excite emitting more x-rays. Johannes Stark was the first to differentiate the two types of x-ray radiation. In 1909 he used Einstein's light-quantum theory to show that the Crookes tubes would fluoresce if the incident electron energy was higher than the outgoing x-ray energy [1].

## 1.2 The Discovery of X-ray Diffraction

Shortly after x-rays were discovered, researchers began working and developing x-rays for medical purposes, as it was quickly discovered that x-rays could penetrate through a person and the 'shadow' could be recorded on a special photographic plate [3]. It was not until two decades later that two physicists first discovered the possibility of x-rays to be used in crystal diffraction. X-ray diffraction was worked on, developed, and implemented by many people.

### *1.2.1 Max von Laue and Paul Peter Ewald's Work*

The beginning of work on x-ray diffraction occurred in 1912 when Paul Peter Ewald met Max von Laue and conceived the idea. Ewald was working on a doctoral thesis, which was to study the 'optical properties of an anisotropic arrangement of isotropic oscillators [4]. Essentially, it was a theoretical model, for crystals, as a lattice of resonating atoms. A crystal lattice, is any ordered, repeating arrangement of atoms. These lattices are typically described in terms of Miller indices, which will be introduced later in this chapter. The distance between these oscillators, however, was a tiny fraction of the wavelength of visible light. At the same time Laue had been working on x-ray research. Laue believed that x-rays were light rays and would be of short enough wavelength to diffract off of the arrangement of atoms [4].

Experiments to test Laue's theory were carried shortly after by W. Friedrich and P. Knipping [1]. They used a series of screens to get a thin x-ray beam which was pointed at a crystal. Behind this sat a photographic plate. Using copper-sulphate they immediately saw many regularly arranged dots on the plate, discovering x-ray diffraction.

*1.2.2 Bragg's Law*

W. H. and W. L. Bragg, father and son, found out about P.P. Ewald and M. Laue's research and began working on theories as to the mechanism of x-ray diffraction. Bragg senior hoped to use x-ray diffraction to show x-ray's dual particle-wave nature. Bragg junior, however, believed that the diffraction was caused by x-ray wave interaction [5]. While these two ideas are now known to be not mutually exclusive, W.L. Bragg's classical approach led to an easier theoretical model. Essentially, x-rays are modeled as waves. They would reflect off varying depths of crystal planes and interfere with each other based on differences in path lengths. W.L. Bragg's theory is what is now known as Bragg's Law and is discussed further in Chapter 2. As all this research was being worked on before quantum mechanics was developed, it is remarkable that a classical explanation of x-ray and crystal interaction proved so successful.

## 1.3 Development of X-Ray Diffraction in Thin Films

Since the discovery of x-ray diffraction in 1912, it has been studied and developed in a number of different ways. X-ray diffraction can be used to determine the structure of most solids. It has been used in everything from metallurgy, which is discussed briefly below, to discovering the structure of DNA by Watson and Crick in 1953 [6].

*1.3.1 Early Diffraction*

W.H. and W.L. Bragg were not just crucial in laying down the theoretical concepts behind x-ray diffraction, they also built an x-ray ionization spectrometer shortly after the discovery of x-ray diffraction in early 1912 [7]. The design of this led to the beginnings of modern diffractometers [8]. Their design produced diffraction patterns by striking a collimated monochromatic x-ray beam onto a crystal. They then placed an ionizing spectrometer at the reflecting x-ray angle. With this they could determine the reflection coefficient at that angle [7]. By varying the angle, they could produce a diffraction spectrum. As with all light, the reflected and incident angle was the same. With this machine W.H. Bragg was able to measure the spectrum of x-rays produced in these crystals while W.L. Bragg applied the information to solve many simple atomic structures such as that of NaCl and zinc-blende the results of which he published in 1913 [9]. World War I, however, delayed this research for several years.

### *1.3.2 Diffraction in Metals*

X-Ray Diffraction in metals began being researched heavily with the development of x-ray powder diffraction independently by P. Debye, P. Scherrer and A.W. Hull [8]. Powder diffraction is an application of Bragg's design. However, in powder diffraction the material is usually ground up. The crystals in the material then are oriented in all directions. This allows for the analysis of polycrystalline substances like bulk metals. The ability to solve the crystal structure of metals and alloys was immediately employed in metallurgical science and allowed for a deeper understanding of the formation of alloys and the crystal shape modification as a result of manufacturing processes. Powder diffraction had many industrial uses specifically in the field of metallurgy [10]. The crystal lattice of a metal could be analyzed after it had undergone various industrial processes. This was already well known by the early 1940s.

Important to the behavior of metal is the internal strain in the metal. This strain is observed as atomic lattice deformations. Lattice distortions give an indication of the strain in a metal or thin film and are important to measure. They are often observed as widening of the x-ray diffraction pattern peaks. W. A. Wood in the 1930s used x-ray diffraction as a method to study lattice distortions like in cold-drawn constantan wire [11]. Lattice distortion measurement with diffraction is also discussed further by N. Kato [12].

### *1.3.3 Thin Film Diffraction*

X-ray diffraction plays a crucial role in understanding the behavior of thin films. As early as the 1930s differences in the crystal orientation of thin, electro-deposited metal films from bulk metals were observed. Wood, mentioned previously, also worked on analyzing the orientations of crystals in thin films compared to the bulk material [13].

With the development of transistors and lasers, the need for a precise understanding of the thin metal films greatly increased interest in x-ray diffraction [14]. In materials like semiconductors, the presence of impurities, also known as the doping of the material, alters the crystal structure of the material. These lattice defects can give rise to free or partially free electrons, changing the electrical conductivity of the material. X-ray diffraction can detect the presence of impurities and can accurately measure the distortions in the lattice caused by them [14].

X-ray diffraction was frequently used in the development of semiconductor materials. For example, J. O. Mcaldin studied the effects of aluminum and arsenic doping in germanium semiconductors using x-ray diffraction in 1959 [15]. Electron transport in zinc-blende materials was studied by C. C. Wang and Leo H. Spinar in 1963 [16].

Reliability in thin metal films is extremely important in the performance of any device using transistors, e.g. any computer. Most thin films fail in response to strain and the ability for them to handle strain changes depending on the film texture [17] [18]. In addition to impurities, the properties of a material can be altered by changes in the orientations of crystals. A single crystal, all the atoms lined up according to a single 3-D lattice, is referred to as a grain. The type and amount of different grains make up the film's texture.

In crystallography, crystals and their orientations are described using Miller indices. A Miller index is based on the reciprocal distance of an atom in a lattice from a corner of the crystal. Thus, the Miller index also varies based on a chosen 'preferred direction'. An example is the face centered cubic crystal shown in Figure 2, where the atoms are positioned on the corners and faces of a cube with sides of length a. The Miller indices define the plane of the crystal parallel to the substrate. Each index is a reciprocal of the point of intersection of the plane of the crystal with the axis. So for the intersection of the blue plane with the three axes: $x = \infty$, $y = \infty$, $x = a/2$. Taking the reciprocals of these, a face centered cubic crystal of this orientation has a Miller index of (0,0,2).

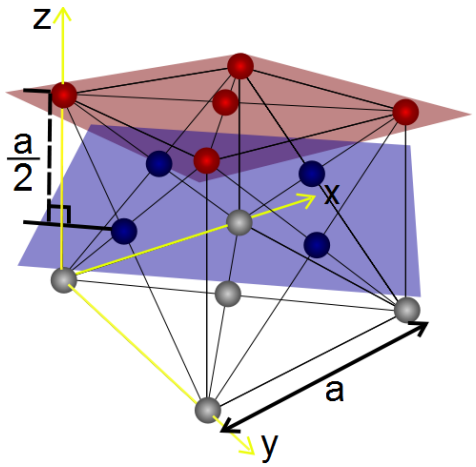


Figure 2. A Face Centered Cubic Crystal. The sides are of length a, and the bottom left corner of the lattice is the origin. Notice that points of intersection of the plane with the axes are $(\infty, \infty, a/2)$ making a (0,0,2) Miller index.

*1.3.4 Development of X-Ray Sources and Optics*

The development of high powered x-ray sources from synchrotron radiation and x-ray beam modification with monochromators and x-ray focusing optics allowed for far more powerful studies of materials with x-ray diffraction [19].

The synchrotron was first planned and built by Edwin McMillan in 1945 at the University of California at Berkeley as a new high energy particle accelerator [20]. While McMillan's synchrotron concept was realized, Vladimir Veksler, unknown to McMillan, was the first to propose the idea in 1944 [21]. Veksler proposed an accelerator which would synchronize a changing electric field with the orbit of a charged particle. Unlike a cyclotron, the synchronization would allow for relativistic charged particle speeds [20].

Synchrotron radiation is caused by the acceleration of charged particles and is produced in abundance at a synchrotron, some of which are developed specifically for this, like the European Synchrotron Radiation Facility (ESRF). It covers a spectrum of energies corresponding to harmonics of a charged particle's frequency of revolution. When the charge particle is travelling at relativistic speeds, the direction of its emitted radiation will become deformed in the direction of the instantaneous direction of motion of the emitting particle, collimating the radiation. In addition, as the kinetic energy of the particle increases, the number of radiation harmonics increases, until a broad 'white' spectrum of light is produced from below visible light to hard x-rays [19] allowing for x-ray diffraction. Starting in the 1970s the scientists began using this radiation for diffraction experiments.

In order to select specific x-ray energies from the synchrotron spectrum, and to further collimate the x-ray beam, x-ray monochromators and focusing optics have been developed [14]. Both use diffraction in crystals of known structure to modify the beam. A monochromator uses a near perfect crystal, like silicon, as a diffraction grating to diffract different energies of x-rays at different angles [19]. Once a specific x-ray energy has been selected, it can be further collimated using focusing optics. These optics function by curved crystals bending x-rays at different angles in different locations in the crystal. This can focus the x-ray beam [14].

The combination of the high intensity of a synchrotron and the ability to focus x-rays allows for an extremely brilliant and highly collimated mono-energetic x-ray beam for high resolution diffraction experiments [19].

## 1.4 Study of Silver Thin Films

Face centered cubic crystals are a common crystal form in metals [8] and are subject to changes in texture. They tend to form in certain orientations and can transition to other orientations during thermal processing [22]. The impetus for transitions between these orientations is not completely understood as it differs from the current model [17].

### *1.4.1 Crystal Structure of Silver*

Silver forms face-centered cubic crystals like the one shown in Figure 3, where the atoms are on the corners and faces of a cube, and it is one of the metals studied for its texture transition [17]. With most

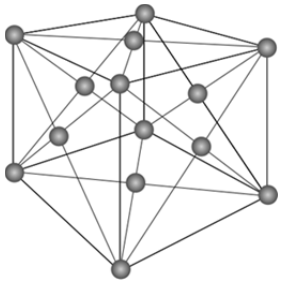

Figure 3. A face-centered cubic silver crystal. The silver atoms can be seen on the corners and the faces of the cube.

deposition processes these crystals form with the (111) orientation with respect to the substrate they are deposited on [23]. The difference between the (200) orientation, which was discussed earlier, and the (111) orientation is that in the (111) orientation, the crystal is stood on its corner. Thus, a line from opposite corners of the cube (between the furthest possible atoms) would be a normal line for the plane of the substrate. The (200) orientation can be seen in Figures 4 and 5 in both a top down and a side view, while the (111) orientation can be seen in just a top down view in Figure 6.

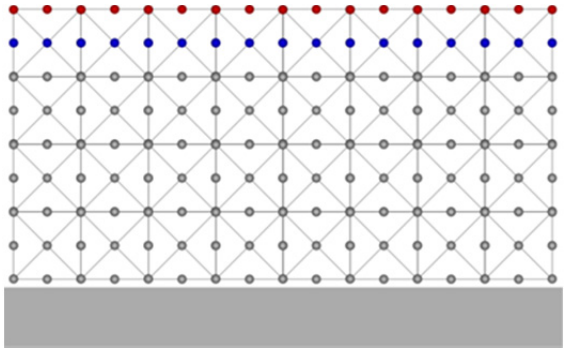

Figure 4. Side view of the (200) orientation. The vertical distance between the repeating planes highlighted by the blue and red colored atoms will form the x-ray diffraction pattern.

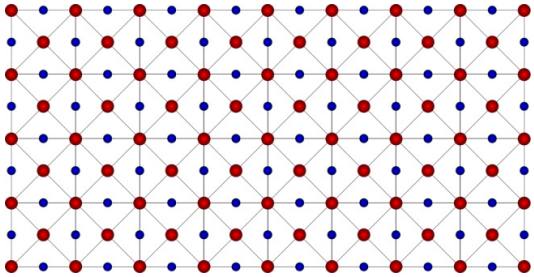

Figure 5. A view of the (200) orientation. The red atoms correspond to the top plane. The smaller blue atoms are the second layer and are formed by the atoms on the face of the sides of the crystals.

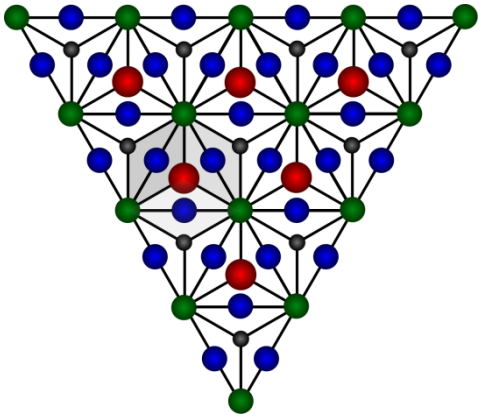

Figure 6. Top view of the (111) orientation. The shading on the cube is to show the contour of the surface. From top to bottom are the red, blue and green, and grey p labeled atoms forming planes that will be observed in the diffraction pattern.

### *1.4.2 Texture Transition in Silver*

The transition of silver between the (111) orientation and the (200) orientation has been theorized to occur as competition between the interface and strain energy [24] [25]. For a give elastic strain, the interface energy per unit volume in the film decreases with the inverse of film thickness, while the

strain energy per unit volume remains constant at a given elastic strain [17]. According to current theory then, there should be threshold thickness of a film below which the (111) orientation dominates and above which the (200) orientation dominates [24] [25].

While the model discussed above is phenomenologically understood, there is not much experimental evidence supporting the interface versus strain energy transition model [17]. In order to test this model, accurate measurements of the stress, strain, and texture over a range of film thicknesses are needed. A decent interface energy estimate is needed as well [17]. This has so far not been done much [24] [26].

In the few studies that have been conducted as discussed above, transitions have been observed to occur well below the threshold given by the standard theory [25] [27] and so much more investigation about this phenomenon is needed.

The transition of silver between orientations can easily be observed with a diffractometer. By Bragg's Law, which is discussed in Chapter 2, differences in distance between crystal spacing will result in changes in the diffraction pattern. The distance between planes in the (200) lattice is from the top of the crystal to the middle face centered atoms. In (111) orientations, the plane distance is from the corner of the cube to the silver atoms on faces adjacent the corner. S. P. Baker et. al. observed the (111) orientation peak and (200) orientation peak at 38.12 degrees and 44.28 degrees respectively [17] with K-alpha radiation from copper, which has a wavelength of 1.5418 Angstroms [28]. This is also a wavelength which could be achieved by the diffractometer, which is the subject of this thesis and it will be discussed further.

## 1.5 Thin Film Research at Houghton College

It is the goal of the materials science lab at Houghton College to develop the equipment necessary and to subsequently investigate the crystal orientation transitions of metal thin films. The lab is developing four main instruments, a deposition chamber, a laser interferometer, an atomic force microscope, and an x-ray diffractometer, which is the topic of this thesis and will be detailed further in Chapter 3.

### *1.5.1 Deposition Chamber*

The deposition chamber is used to produce the thin films for research in the lab. It consists of a large aluminum chamber which pumped down to high vacuum. Inside the chamber a small crucible of

metal is heated by bombardment by electrons produced in a filament. The metal ions then evaporate and will accumulate onto a silicon disc in the chamber. Inside the chamber is an evaporation rate monitor which allows films to be made with a predetermined thickness. This then can create very thin metal films. It is currently designed to produce thin films of silver. The chamber is still under construction and will hopefully be finished soon.

*1.5.2 Laser Interferometer*

The laser interferometer uses the reflection and interference of laser light to measure the topography of the films. The measurement of the topographical warping can reveal the stresses of the film. With a stepped thickness film, the interferometer can also measure thickness while the film is being deposited. It will be mounted to the finished deposition chamber and the laser light can be directed through a small window into the chamber. Any change in the curvature of the film is the result of stress and can be measured with the interferometer.

*1.5.3 Atomic Force Microscope*

The atomic force microscope uses a very thin needle probe which runs across the surface of the film. Atomic electromagnetic forces push the needle up and down. Laser light then reflects off the top of the needle arm and is used to measure the minute atomic scale deflections of the needle.

The atomic force microscope gives detailed information on the surface of the film. This can give a picture of the roughness of the surface of the sample. This specific look and roughness of the surface can give an idea of the crystal orientations of the sample. Islands of specific crystal orientations can then be observed as they form and coalesce with each other.

*1.5.4 X-Ray Diffractometer*

The x-ray diffractometer is critical in determining the atomic lattice spacing of the thin films studied in the lab. A diagram of this diffractometer is shown in the Figure 7. A collimated x-ray beam is directed at the target sample where the sample is oriented at an angle theta from the incident x-rays. Some of the x-rays will diffract off of the sample and are collected by the x-ray detector. As a result of the geometry of Bragg's law, the detector is placed at twice theta measured from the incident x-ray beam line.

These diffraction patterns will correspond to the atomic plane spacing in the crystal. The distance between these planes is caused by different crystal orientation. In addition to plane spacing, the diffractometer can pick up any high concentration impurities in the silver. During the deposition process, some of the silver can oxidize and other crystals will be in the film. In a high enough concentration these will alter the plane spacings significantly which can be identified as well. If an energy resolving detector was used, impurities could also be identified by their x-ray fluorescence.

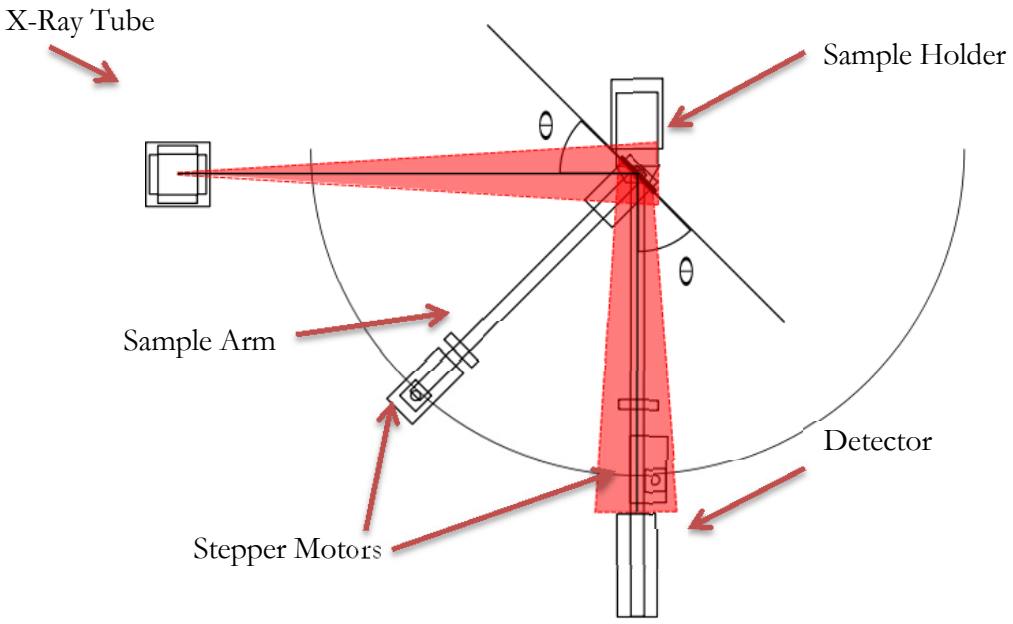


Figure 7. Diagram of a Bragg-Brentano Diffractometer. This is the design of our specific diffractometer. The divergent x-ray beam strikes the target, which is rotated by the sample arm, and diffracts. The detector arm is positioned at twice the angle from the beam as the sample, centering the detector on the diffracted x-rays. The angle theta is the angle used in Bragg's Law for determining locations of constructive interference.

*Chapter 2*

# THEORY

## 2.1 X-Ray Diffractometer Theory

In the construction of an x-ray diffractometer, a few theories, discussed below, are important for the development of an apparatus. The diffraction patterns produced by the diffractometer can be understood in the context of Bragg's Law. Crucial to understanding the pattern is also understanding the components of the x-ray energy spectrum produced in the x-ray tube, which is discussed in terms of fluorescence and bremsstrahlung radiation.

## 2.2 X-Ray Production

X-ray production for this experiment is accomplished by an x-ray tube. These function by an electron being accelerated into an elemental target material. The interactions between the two produce x-rays in two main ways, bremsstrahlung and fluorescence.

A typical x-ray radiation spectrum produced by an x-ray tube consists of a broad, smooth, 'white', spectrum caused by bremsstrahlung with several sharp peaks from x-ray fluorescence of the target. Both are significant components of the spectrum. However, the sharp peaks of the target fluorescence allow for determination of the diffraction spectrum, and so, must be well understood.

### *2.2.1 Bremsstrahlung X-Rays*

Bremsstrahlung x-rays are caused by the sudden acceleration of electrons as a result of conservation of energy [7]. In the x-ray source, electrons are accelerated from rest towards the grounded anode by a high negative electric potential, up to -50 kV for this system. The incident electron energy can then be calculated as:

$$E_{final} = E_{initial} = KE + PE. \quad (1)$$

$$KE_{initial} = PE_{final} = 0,\ PE_{initial} = KE_{final} = q\Delta V, \quad (2)$$

where KE is the kinetic energy, PE is the potential energy, $q$ is the charge of the electron, and $\Delta V$ is the change in electric potential between the target and the cathode. Upon reaching the target the electron will strike the nuclei in the metal. Each interaction an electron undergoes with a nucleus in the target changes the electron's energy, causing the emission of x-rays. The maximum energy x-ray produced would be as a result of the electron striking the atom and immediately coming to rest,

$$v_o = \frac{q\Delta V}{h}, \quad (3)$$

where $v_o$ is the maximum frequency (highest energy) for an x-ray and *h* is Planck's constant [7]. A more glancing interaction, however, would result in a lower energy x-ray emitted, and the electron travelling on to interact further. The energy spectrum of bremsstrahlung x-rays is broad. It extends from the maximum, an accelerated electron stopping in one collision, down to the minimum energy of an x-ray. The bremsstrahlung x-ray curve is primarily a function of two things: the probability of an electron of a given energy interacting and the probability that an emitted x-ray is absorbed before it exits the target. As a result of the continuous energy distribution, this would not produce any distinguishable diffraction lines.

*2.2.2 X-Ray Fluorescence*

X-ray fluorescence is caused by atomic ionization followed by an outer shell electron de-excitation. Figure 8 shows the basic mechanics of it. When an electron strikes the anode it can lose some of its energy to removing an inner anode electron. An outer atomic electron will then de-excite to fill the gap and emit a photon with the energy of the corresponding energy level change. This process occurs in the same way as optical fluorescence with the exception that these emitted photons are significantly higher energy.

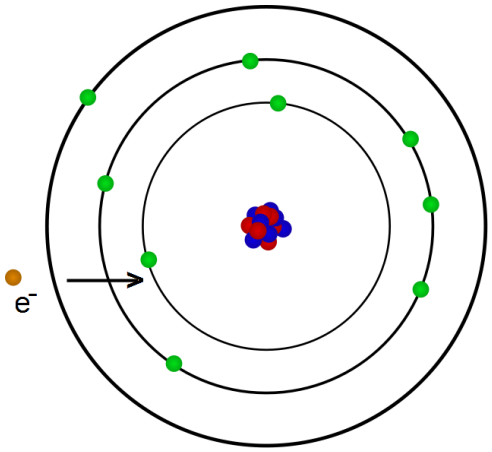


Figure 8. Fluorescence dynamics with the Bohr model. The incident (gold labeled) electron removes a (green labeled) atomic electron, opening a spot for a higher energy electron to move to a lower energy.

Multiple fluorescence x-rays are possible as long they have an energy less than or equal to the incident electron. X-ray fluorescence will occur as long the incoming electron energy is high enough in energy to remove an inner atomic electron. In Figure 9 an example energy band gap of 25 keV is given. Target materials can then be chosen which produce a wanted discrete x-ray spectrum. Since x-ray fluorescence produces significant amounts of certain energies of x-rays, each x-ray energy will produce a detectable diffraction pattern.

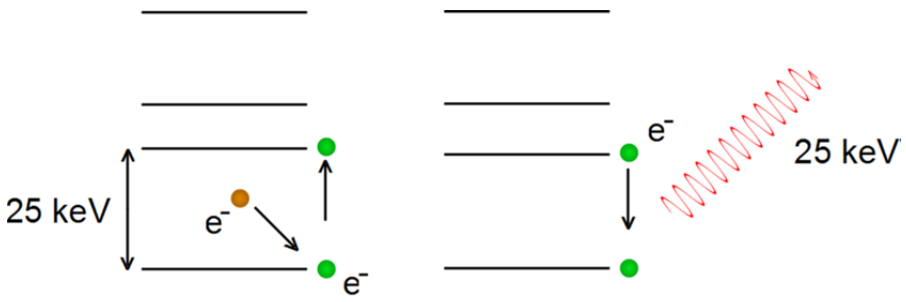


Figure 9. Band gap transitions in fluorescence. The incident (gold labeled) electron collides with an atomic electron giving it enough energy to leave. An outer atomic electron then de-excites and 25keV is released as an x-ray.

Specific x-ray fluorescence energies are referred to based on the energy level transition taking place. $K_\alpha$ and $K_\beta$ are fluorescence energies that are typically seen at the energies we will be using and correspond to transitions to the innermost electron shell, where the shells are K, L, M, and N, innermost to outermost. $K_\alpha$ corresponds to transitions from the L level to the K level. $K_\beta$ corresponds to transitions from the N and M levels to the K level.

## 2.3 X-Ray Diffraction

### *2.3.1 Bragg's Law*

Bragg's law gives a theory for the interference pattern of x-rays diffracted off of a crystal. It was developed by William Lawrence Bragg as a simpler approach to x-ray diffraction than Max von Laue's analysis, which is based on a three dimensional diffraction grating. Bragg saw diffraction as the reflection of x-rays by crystal planes. The difference in path length that an x-ray would travel when it is reflected on a deeper plane would lead to constructive and destructive interference of the x-rays.

An x-ray can be classically modeled as an electromagnetic wave. For the sake of simplicity, this wave can be written as

$$A(x) = \sin(\omega x + \delta), \tag{4}$$

where, $A(x)$ is the amplitude of the wave at position $x$. The wave has a frequency of ω and a phase shift δ.

Two identical waves coming from an x-ray source can then be considered. Figure 10 is an example of this. These waves, if close enough, will add together and be observed together interfering:

$$A_{total}(x) = \sin(\omega x + \delta_1) + \sin(\omega x + \delta_2). \tag{5}$$

This sum can be simplified with a Sum-to-Product identity.

$$A_{total}(x) = 2\sin\left(\frac{(\omega x + \delta_1) + (\omega x + \delta_2)}{2}\right)\cos\left(\frac{(\omega x + \delta_1) - (\omega x + \delta_2)}{2}\right). \tag{6}$$

$$A_{total}(x) = 2\cos\left(\frac{\delta_1 - \delta_2}{2}\right)\sin\left(\omega x + \frac{(\delta_1 + \delta_2)}{2}\right). \tag{7}$$

So, the sum of the interfering waves is an oscillation between constructive and destructive interference, the cosine term, with a sine wave of the same frequency as the two constituent waves and an averaged phase. For constructive interference, as in Bragg's Law, the cosine term must be at a maximum. This will occur when

$$\frac{\delta_1 - \delta_2}{2} = 0, \pi, 2\pi, \ldots \tag{8}$$

or,

$$\Delta\delta_{12} = 0, 2\pi, \ldots = n\lambda. \tag{9}$$

In the case of x-ray diffraction, the change in phase occurs due to a change in the path length travelled by the wave. In Figure 10 it can be seen that the additional path length can be calculated from the distance between two subsequent planes, and the incident angle of the x-rays. The additional path length is twice the length of each gold line segment. If this path length is equal to an integer multiple of the wavelength, constructive interference will occur. This condition gives rise to Bragg's Law:

$$n\lambda = 2d\sin\theta. \tag{10}$$

Since x-rays are highly penetrating, they will diffract off of all the layers in the thin film material. As a result of this, the reflected x-ray intensity does not vary as it would with only two layers. It will have sharp peaks at the location of constructive interference, given by Bragg's Law, and almost no signal elsewhere. This is caused by the addition of a large number of reflected waves, since the thin film acts as a many slit diffraction grating, just like an optical diffraction grating does [29].

Bragg's Law can then be used to determine the texture of the film, or, how much of it is a specific crystal orientation. The relative intensity of the diffracted x-rays at a given Bragg angle depends on the total amount of the film which has the orientation interfering constructively at that angle versus the integrated intensity of the reflected x-rays. With this, the percentage of the film that has a specific orientation can be found.

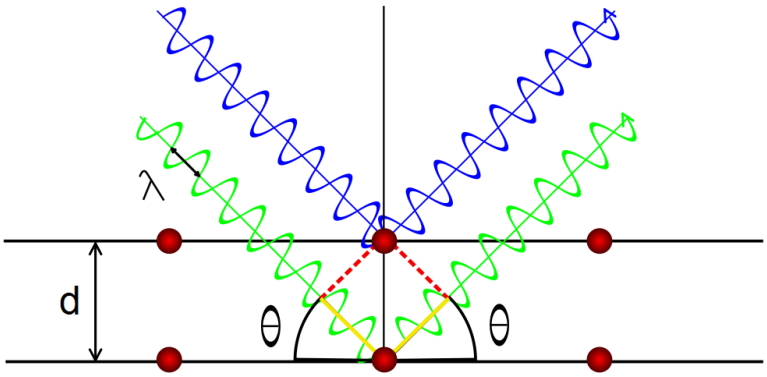


Figure 10. Bragg's Law diagram. The variables in Bragg's Law are displayed. As can be seen in this example, the incident coherent x-rays are destructed at the shown angle. Unlike in the above equation, this would correspond to half integer multiple n. The gold line corresponds to the additional path length travelled by the green wave.

*Chapter 3*

# APPARATUS

## 3.1 An X-Ray Diffractometer at Houghton College

The construction of an x-ray diffractometer is crucial to research on thin films at Houghton College. In this chapter, the specifications and design of the College's diffractometer are described in detail. The diffractometer, for organization purposes is divided into four main components, the x-ray system, the mechanical system, the electronic system, and the detection system.

## 3.2 The X-Ray System

### *3.2.1 The Old X-Ray System*

An old x-ray machine at Houghton College was used as a starting point for building the diffractometer. It contained useful components which would be very difficult to manufacture and very expensive to purchase. The old x-ray diffraction system was built by Philips-Norelco in the late 1960s. Not much is known about it, other than that at one time it is believed to have been used in the lab, and when it was found, hadn't been used in many years. It consisted of a high voltage power supply and several x-ray tubes. The diffraction system was largely gone or disassembled. Much of the model was not working when it was found and the working parts were salvaged and the rest scrapped. The scrapped parts are in Figure 11 on the next page.

The cooling system for the x-ray system and power supply were determined to be completely non-functioning and were scrapped. The x-ray tubes that were used in the old system were intact and did produce x-rays when connected to temporary lower powered setup which will be discussed later. The column that holds, shields, and provides water cooling for the tubes also worked and was kept.

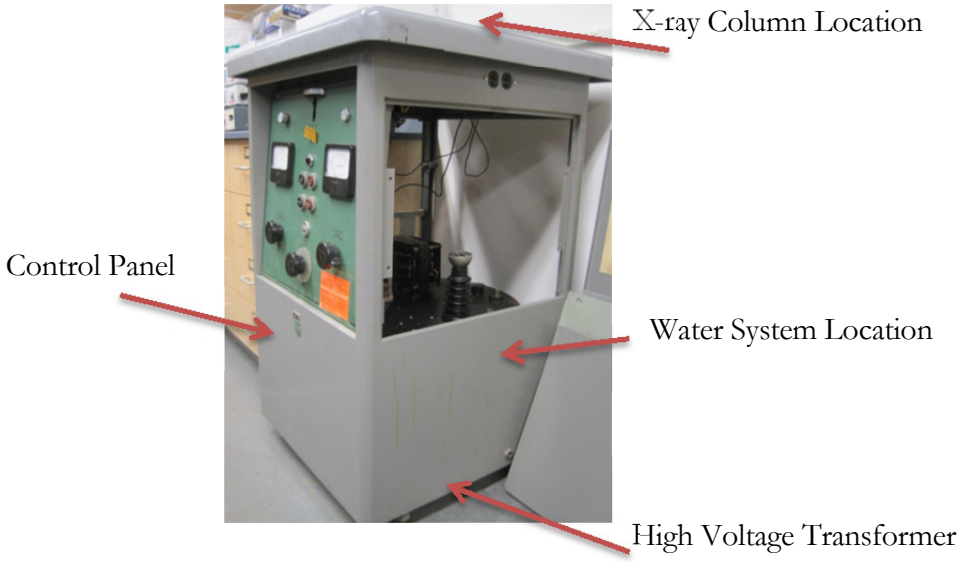


Figure 11. The old non-functioning x-ray system. The x-ray column cannot be seen as it has been removed. In addition the water system has been removed. Remaining is the black oil cooled high voltage power supply in the bottom and the front control panel. This shows the discarded part of the system.

*3.2.2 The New X-Ray System*

The rebuilt x-ray system consists of a lab table on which the diffractometer apparatus and x-ray column sit. It can be seen in Figure 12. Underneath, the high voltage system and electronic controls, including a computer console, sit.

The x-ray column is from the old system and is bolted to the table top. A diagram of the inside of the x-ray tube, which sits in the column, is shown in Figure 13. The column has four horizontal ports through which x-rays from the tube are emitted. With the ports closed the emitted x-ray radiation is not perceivable above background. The column also provides an outgoing and incoming cooling pipe for the x-ray tube. The grounding of the x-ray tube, important for electron transmission, is also through its attachment to the column.

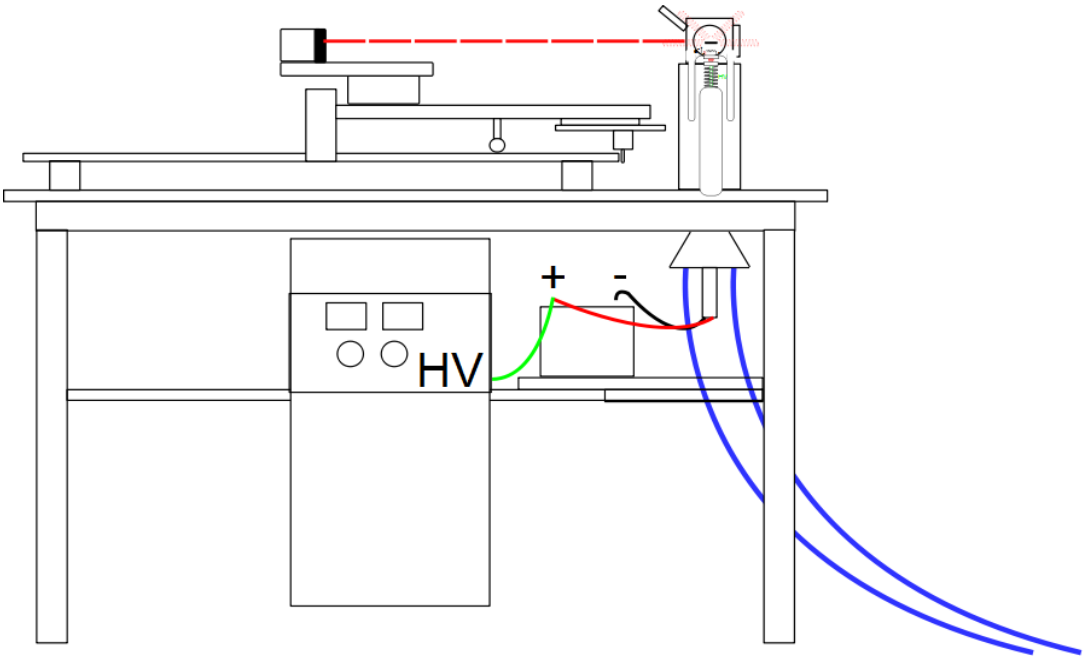


Figure 12. Diagram of the new x-ray system. The water system pipes are labeled blue and run to a sink in the lab. The red black and green lines are wires in the filament circuit, not shown is the large power resistor. Above, in the x-ray column, a small x-ray tube can be seen with the red dotted line being the x-rays escaping from the open port towards the sample holder.

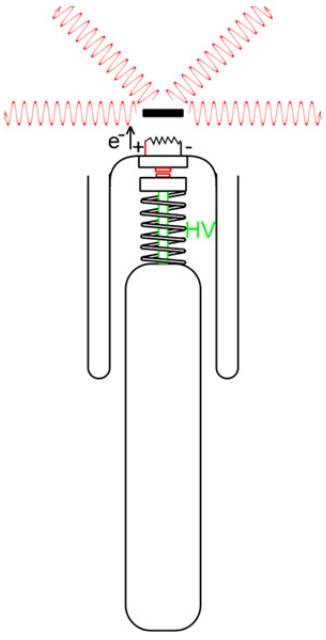


Figure 13. Diagram of the x-ray tube. This is a cross-sectional view inside the x-ray tube with the high voltage post inserted. The post contacts the tube where the two red discs meet. This heats the filament and brings it to a high voltage. Electrons produced through thermionic emission are accelerated towards and strike the target shown, producing x-rays.

The x-ray tubes are from the old setup and if broken would be very difficult, if not impossible to replace. They are also the only tubes compatible with the old column. A high voltage post is placed inside the tube where the inner and outer rings on the high voltage post differ by a few volts in order to heat the filament in the tube. Once the filament is heated, the high negative voltage of the post causes electrons thermally emitted from the filament to accelerate towards a grounded target in the tube. If the energy of the accelerated electrons is high enough to free an inner electron in the target, the target will begin to emit x-rays produced through fluorescence. These will have a specific energy dependent on the target material. We have copper, cobalt, chromium, and molybdenum target tubes. The fluorescence x-rays produced are shown in Table 1.

| | K-alpha (Angstroms) | K-beta (Angstroms) | Excitation Potential (kv) |
|---|---|---|---|
| Copper | 1.5418 | 1.39217 | 8.86 |
| Cobalt | 1.7902 | 1.62073 | 7.71 |
| Chromium | 2.2909 | 2.08479 | 5.98 |
| Molybdenum | 0.7107 | 0.63225 | 20.0 |

Table 1. K alpha and beta emission. This figure shows the K-alpha and K-beta x-ray wavelengths and excitation potentials for the targets: Cu, Co, Cr, Mo. These are in the x-ray tubes being used at Houghton. Table taken from Ref. [28].

While x-rays will be produced in any electron-target collision, typically bremsstrahlung radiation, these will be of a broad spectrum of energy. From Bragg's Law, a given diffraction pattern is produced at a specific energy of x-ray. Thus, x-rays from fluorescence will produce a distinguishable signal.

The power system for the x-ray tube is much simpler than the old system, as it doesn't require an external cooling source. It is also smaller and less powerful than the old system. The circuit for the new system is shown in Figure 14 on the next page. It will be temporary though, as it used in other parts of the lab. It is, however, quite sufficient for x-ray production and is useful in preliminary system testing. The high voltage power supply uses 120 VAC power from the wall and produces 0 to -30 kV DC at up to 12 mA. This is in contrast to the old power supply which at one time could have produced up to -50 kV and 50 mA. The filament current in the new system is supplied using a 12 V car battery. The benefit of a car battery is that it can float at the necessary high voltage without shorting out like a grounded power supply would. Among batteries, it provides a high power output and is easily

recharged. The current flow through the filament is controlled by a large, 8 Ω maximum, variable power resistor in series with the 0.5 Ω filament. Since the water cooling system is now no longer needed for the high voltage supply, it is only used to cool the x-ray tube and column assembly.

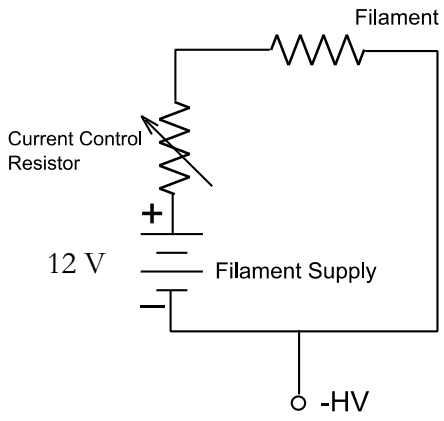


Figure 3. The filament circuit. The circuit above shows the current configuration of the filament circuit. The variable current control resistor can be seen in series with the filament and filament power supply. Not shown is the grounded target above the filament which causes a small current from the –HV.

Since there was no manual for the old x-ray system, nothing is known about the cooling needs of the x-ray tube etc, other than the fact that they were cooled, obviated by the cooling pipe running through it. Currently the cooling pipe is hooked up to a lab sink with rubber hoses running in between. The current flow rate limitation is due to the ability of the rubber hoses to seal to the pipes on the x-ray column. However, during operation no change in temperature from the incoming and outgoing cooling water has been measured. So, it is assumed the cooling needs are being met. This setup is also temporary and will be replaced once a closed water system with a chiller is constructed.

*3.2.3 Shielding and Beam Collimation*

In order to reduce background radiation and reduce the x-ray beam width, a collimation system will be designed. This part of the x-ray system is still under development but will be crucial to improve data quality. Due to the large angular spread of the x-ray beam, a collimator near the sample will be used to significantly reduce beam spread. In addition, the rest of the diffractometer will be shielded from the divergent beam, significantly reducing background from scattered beam x-rays. An additional collimator will be placed in front of the detector with shielding around it. This will constrain the detector's x-ray acceptance to only the direction of the incident diffracted x-rays, reducing background.

### 3.3 Mechanical System

The mechanical system has been completely designed and built at Houghton College. The basic design of the diffractometer is of the Bragg-Brentano type. It has a large half circle disc which forms a track for two arms to rotate. One arm rotates the sample, and the other rotates the detector. The rest of the system is built to house the remaining parts of the apparatus and necessary electronics as well as shield the lab from the x-rays produced.

#### *3.3.1 The Table*

The table's primary function is to house the diffractometer and its peripheral systems. On the top of the table sits the diffractometer apparatus which is shown in Figure 15. Underneath, sit the power supply, the motor control system, and the computer console along with shelves for necessary spare parts during construction.

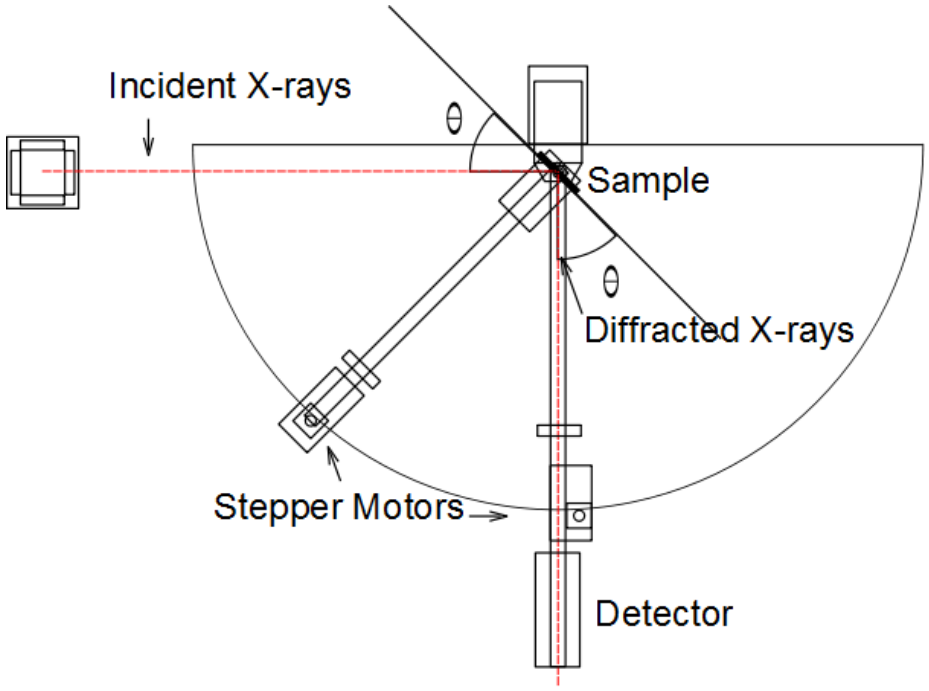


Figure 4. A top down view of the diffractometer design. The major components of the diffractometer are labeled in the above figure. The red dashed line shows the center of the x-ray beam, which is divergent. The angle theta corresponds to the angle in Bragg's Law.

The half circle is mounted to the table on top of four 2 x 2 inch aluminum blocks. The circle itself is 18 inches in radius and made of ½ inch thick 6061 aluminum. The center of the circle has a ½ inch diameter hole drilled and an aluminum rod press fit into it. This forms the pivot for the two arms in the apparatus to rotate about. The center of this hole is directly in line with the center of the x-ray beam. On the top of the rod another plate is fastened which ensures the rod remains vertical even with the weight of the arms attached to it.

The half-circle was cut with great precision and differs from a perfect circle by approximately 1/64 of an inch. The cut aluminum surface is smooth and consistent except for minute ridges caused by the mill bit used. The traction surface for the motors will likely be covered in fine grain sand paper to both reduce the ridges and add traction for the motors.

*3.3.2 The Arms*

The arms rotate the sample and detector about the center of the circle. They are drilled through on the rotating end with a bearing mounted to it, allowing the arm to mount to the rod. The bearing fixes to the rod with a lock-screw. The sample arm is fastened directly above the detector arm so that it can have a sample holder attached above it. Each one has a 1 x 1 inch square cross section and is also made of 6061 aluminum. In order to balance the arms and bear some of their weight, to limit force on the bearings and motors, two casters are attached underneath each arm. These roll on top of the circle with the arm's track of motion. The end of each arm has a motor mount attached. These mounts use four 50 mm long #3 metric bolts which thread into the stepper motor case.

The sample arm is shorter and higher than the detector arm. A diagram of it is shown in Figure 16. A half inch hole is drilled through the center of the arm, through which is a half inch diameter threaded rod. This rod bolts to the arm and bolts to a 1/8 inch aluminum plate underneath. The casters to support the arm bolt to this plate. This design allows the height of the arm to be adjustable and provides a stable platform for it to rest on.

The motor mount for the sample arm extends a small amount beyond the length of the arm. The motor itself is mounted to a ¼ inch plate which has two inline, ¼ inch wide slots to bolt to the arm. This plate hangs under the arm by a further ¼ of an inch by a small spacing plate, which moves the top of the motor to ½ of an inch under the top arm.

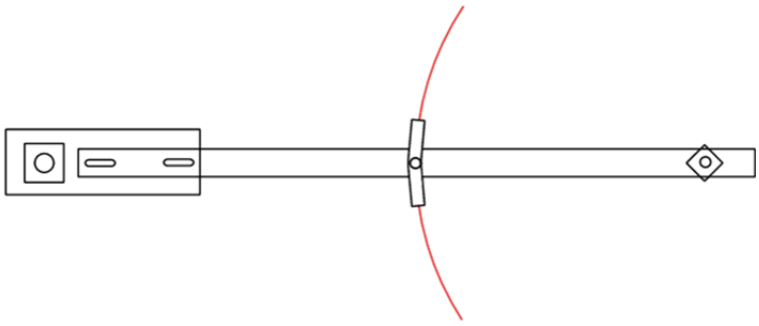

Figure 5. A top view of the sample holder arm. On the left the motor can be seen mounted under a plate. This plate mounts underneath the arm with two bolts. The slots for these can be seen on the arm. Mid-figure the casters and their arc of motion is shown. On the far right is the bearing and the hole where the arm fixes to the axle.

The bottom detector arm is much longer than the top arm. Since detector system has not been decided upon, making the arm longer left more room for options and provided greater flexibility for how close or far the detector can be mounted. As a result of the bottom arm being so close to the aluminum half-circle plate, significantly different designs were necessary for the motor mount and the caster mount. A small 3 inch long rod was cut from the same rod as the arms and used to mount the casters. Half of the thickness of the rod was milled out and it was bolted to the top of the arm, through the center, with a ½ inch threaded rod. Small holes were then tapped at an angle into the bottom of the arm for the caster mount machine screws to thread into.

The motor mount for the detector arm actually positions the motor alongside and flush with the arm. A diagram of it can be seen in Figure 17. A ¼ inch thick plate is used as the structure to fasten the motor and arm together. Two 1 inch long, ¼ inch wide slots are cut into the plate next to the motor

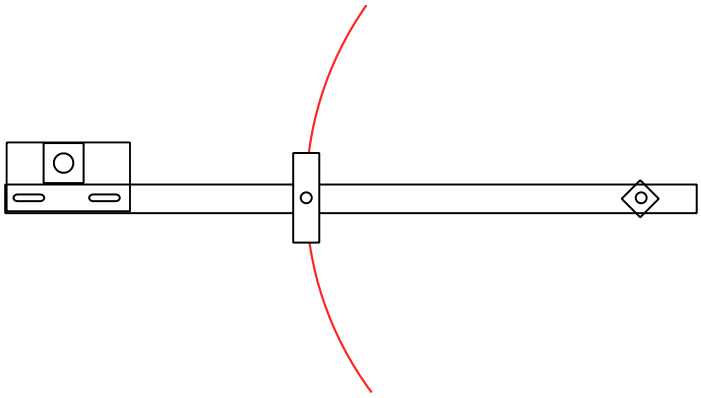

Figure 6. A top view of the detector arm. The motor mount can be seen in the left part of the diagram. Here, the back of the motor is at equal height with the top of the arm. In the middle are the casters along with the arc that they travel. Far right is where the arm mounts to the axle

mounting holes. These slots then fix the plate to the arm and adjust in and out to make the motor installation easier. The motor sits flush with the arm and is mounted through the top with four #3 metric bolts just like the sample holder arm motor mount.

This system requires a great deal of adjustment to function smoothly. The casters are currently not perfectly aligned with the arc of the circle and after a short distance of travel begin to bind against their axles. Lock washers are in place in order to prevent slippage but, a great deal of tweaking is still required.

### *3.3.3 The Motors*

The motors are small stepper motors which provide a great deal of angular accuracy for the system. They have small D-shaped metal axles. On each corner of the top of the square case of the motor is a small hole through which small #3 bolts thread holding the case together. These were removed and replaced with longer bolts which allow the motor to mount to a ¼ inch plate as well; the bolts now running through both the plate and the case. For the axles, a small rubber hose fits around the outside giving it greater traction on the aluminum track. They also round out the D-shape to an extent, though this needs improving.

## 3.4 Electronic System

The electronic control system for the diffractometer currently consists of two separate systems: the LabVIEW system and the LoggerPro system. The LabVIEW system provides control for the electric motors. The LoggerPro system is purely for quick data collection and is used for radiation monitoring and water system temperature monitoring. Since there is no way to link LoggerPro data with motor position, or any other LabVIEW data, LoggerPro's function will need to be replaced by LabVIEW. Both systems run on the computer console in the diffractometer table.

### *3.4.1 LabVIEW*

LabVIEW provides a great deal of versatility for data input and analysis as well as apparatus control. A LabVIEW program was written that had been designed and built to run both stepper motors for varying times and distances. This will form the core of the future diffractometer program, which will collect and process the detector signal as well. The computer console has a special PCI card which

runs a National Instruments stepper motor control system, which can drive up to two small stepper motors, perfect for our application.

### *3.4.2 Logger Pro Test Setup*

For the x-ray radiation data and the water temperature sensing, Logger Pro was used. Logger Pro was quick to setup and was being temporarily used for any needed data collection. Two Vernier Student Radiation Monitors were being used: one of which was placed 20 cm away and on-axis with the open x-ray port, and a second radiation monitor was used to measure background radiation in the lab. This one was placed approximately 5 m away at a desk in the lab near the door. The water temperature sensing system had two Vernier temperature probes. One probe was inserted into the rubber hose near the inlet to the short copper x-ray column cooling pipe; the other probe was inserted into the hose just downstream of the x-ray column cooling pipe outlet. The temperature difference measured by these probes was monitored in Logger Pro with the assumption that little or no temperature difference meant the cooling was effective.

## 3.5 Detection System

In the initial verification of the working of the x-ray system, the detection system setup was not very sophisticated and certainly will not be used in the final diffractometer design. The Student Radiation Monitors provided an excellent way of recording radiation produced by the machine over a long period of time, like in the background measurement, and measuring relative changes in x-ray intensity at different filament currents and high voltage levels.

The final system will need to have an energy resolved detector. This will reduce background noise from scattered x-rays and ambient radiation. In addition, sample purity could be measured by analyzing the fluorescence spectrum of the sample thin film.

*Chapter 4*

# RESULTS

## 4.1 X-Ray and Electronic System

The current x-ray and electronics systems run sufficiently for a proof of concept of the diffractometer. With the new, smaller, high voltage supply, the x-ray tubes were tested and produced significant amounts of x-ray radiation. The electronic system is able to operate motors and collect rough radiation output data using a combination of Logger Pro and LabVIEW.

### *4.1.1 X-Ray System*

The x-ray system has been tested with the new high voltage power supply and filament heating system. In order to test the system, the power resistor was adjusted and the filament current was slowly increased and measured on a multi-meter. Once the resistor was adjusted, the high voltage power supply was turned on and brought up to its maximum voltage of -30 kV. The radiation output was then measured at different distances and angles with a Student Radiation Monitor and a survey meter. The following charts show the x-ray production on-axis at different distances and currents. At the closer distances the x-ray production was unable to be measured at higher filament currents as the survey meter and Student Radiation Monitor were unable to record that high.

The data for the three distances recorded are shown in Figures 18, 19, and 20. These measurements were taken with a held survey meter at 0.2, 2.5, and 3.0 meters, respectively, away from the x-ray port and on-axis. Since the survey meter was held and moved by hand, the position it was from the source has an uncertainty of approximately a tenth of a meter and an angular uncertainty of five degrees. It was not possible to calculate the radiation uncertainty given the units of mRem/hr, nor did we calculate the filament current uncertainty.

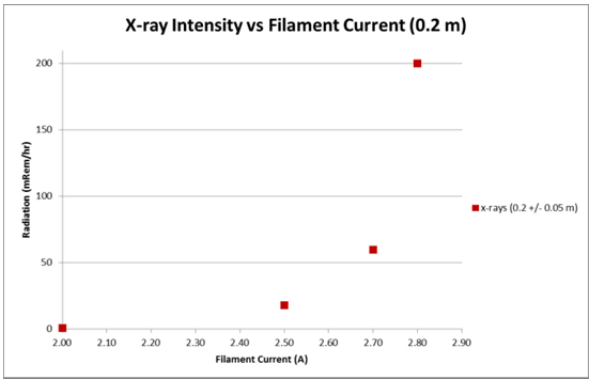


Figure 7. Radiation versus filament current at 0.2 m. This data was taken with a handheld survey meter. There is a distance uncertainty of 5cm.

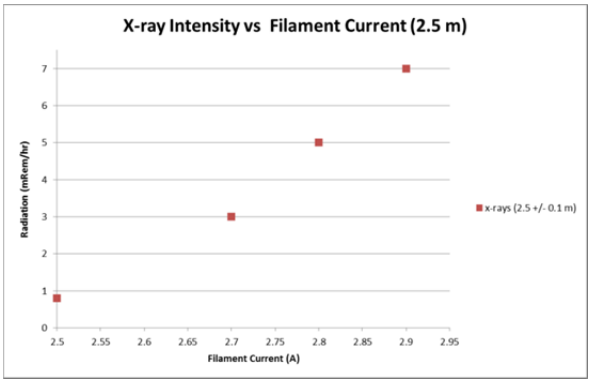


Figure 19. Radiation versus filament current at 2.5 m. This data was taken with a handheld survey meter. There was a distance uncertainty of 10cm.

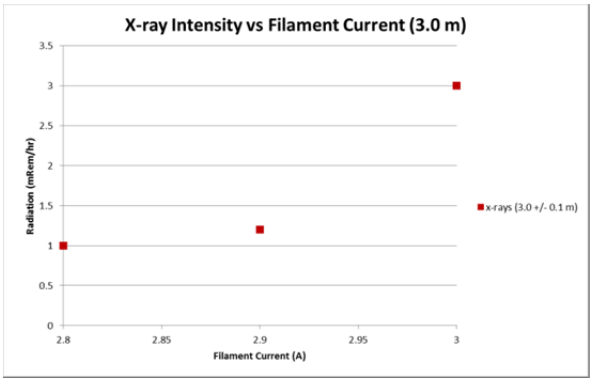


Figure 20. Radiation versus filament current at 3.0 m. This data was taken with a handheld survey meter. There is a distance uncertainty of 10cm.

The maximum filament current tested was 3 A. In addition to testing the radiation on-axis, select horizontal angular measurements of radiation were taken with filament currents of 2.7 A and 2.9 A. The angle was measured between the center of the x-ray beam line and the survey meter. This gave a rough idea of the behavior of the spreading of the x-ray beam. The graph of this data is in Figure 21.

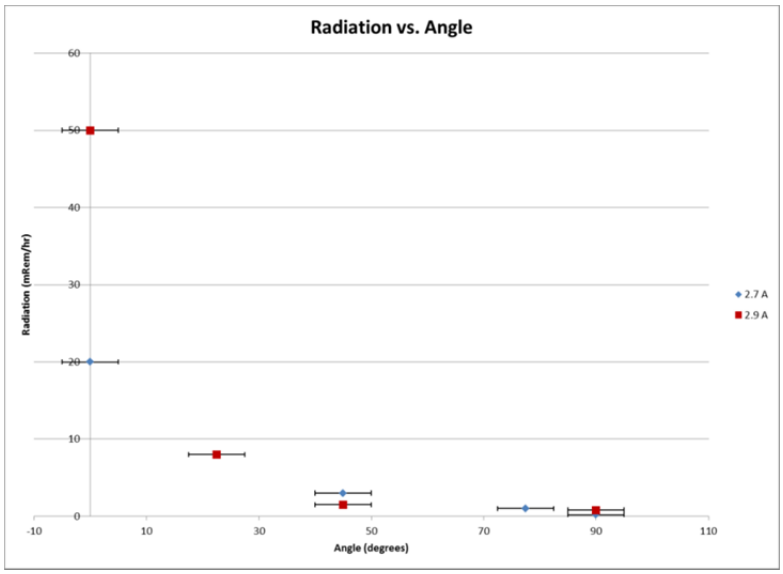


Figure 21. Radiation versus angle. This data was taken with a handheld survey meter. There is an angular uncertainty of 5 degrees.

No diffraction tests have been done yet. Without one, the amount of x-ray radiation necessary to perceive a diffraction pattern would have to be calculated based on the probability of x-ray reflection and compared to background radiation

*4.1.2 Motor Control*

The motor control system has been tested. Both motors can run simultaneously at different programmed rates. The angular change for each arm is related to the distance between the axle the arm rotates about and the motor and the radius of the motor wheel. The radius of the motor wheel is 5/32 inch. The distance between the arm's center of rotation and the center of the motor's wheel is 18 and 5/32 inches. The angular speed of the arm is then related to the angular speed of the motor by the ratio of the distances. This gives excellent angular precision.

$$\omega_{arm} = 0.0086\omega_{motor}.$$

For example, one motor step, 1.8 degrees, would correspond to a .016 degree rotation in the arm.

*Chapter 5*

# CONCLUSION

## 5.1 X-Ray Diffractometer

The x-ray diffractometer at Houghton College is very close to being complete as a proof of concept. With beam collimation, shielding and a sample mount, as well as minor adjustments to the mechanical system, this diffractometer will be ready to collect its first diffraction data. Further refinements, like an energy resolved detector, will be important to improve data quality and increase the diffractometer's usefulness to thin film research.

## 5.2 X-Ray System

The Houghton College x-ray system has undergone extensive revamping since the old system and is currently fully capable of x-ray production. With the current system, initial tests of the feasibility of x-ray diffraction with the apparatus can be performed, which, is a good step forward in building the x-ray diffractometer. Many improvements to the system may be needed and should be the subject of future study.

The current x-ray system is fully capable of producing a large flux of x-rays with energy up to 30 keV. The filament heating system, while not quickly adjustable, should produce plenty of power even with future system upgrades. A more sophisticated x-ray detection system which can resolve x-ray energy will be needed to analyze the x-ray spectrum currently produced. The ability to resolve x-ray energy will also decrease background rates and allow for sample impurity fluorescence measurements.

A working beam collimation system will also be important in the continued refinement of the x-ray system. This, combined with an energy-resolved detector will greatly improve signal quality. Testing of the penetration of the x-rays produced will allow for the determination of the necessary material and thickness in order to successfully shield and collimate the x-rays.

### 5.3 Mechanical System

The mechanical system is almost complete. Much of the apparatus has been built, however refinements and adjustments to the design need to be done. This will require time and testing as the rest of the systems become functional and the different parts of the diffractometer can be tested together.

#### *5.3.1 The Table*

The table itself is mostly done being built. As the final diffractometer components are chosen, some refinements may be needed to fasten the system together. The design of the table should lend itself to being easily modifiable as various component systems need.

Some future work has become needed now that the x-ray system is functional, which until recently it was not. An electrically insulating plastic box to place the filament circuit and power supply in should be added for safety. The mount to the frame for this was built, but the box was not. In addition, a metal box of sufficient density or thickness to stop the produced x-rays will need to encapsulate the top of the table to prevent x-ray radiation leaks. With the recently measured radiation levels, this box will be needed before higher power x-ray tests are completed.

#### *5.3.2 The Arms and Motors*

The construction of the arms is completely finished. The motor mounts and caster mounts have also been fixed on. The motor mounts are physically completed as well. Its current state is very close to being ready for preliminary diffraction tests.

This system does need a great deal of adjustment, however, for smooth running. The thin rubber hose, or 'tire', around the axle should provide sufficient traction once fine grain sand paper is glued on to the track. However, the D-shape of the motor axle causes tight and loose spots along the track as the motor rotates. A small partial circle insert will likely be needed to remove the D-shape and ensure smooth running. A thicker rubber 'tire' could also be used to allow for more rollover ability, reducing the effect of small changes in radius of the motor track.

The mounts for the detector and sample holder will be needed soon. The detector mount has not been designed since a detector has not been chosen. The sample holder mount has been designed and needs to be built to allow for future testing of the diffractometer.

### 5.4 Electronic System

The framework for the electronic system has been completed. LabVIEW is running on the diffractometer computer and a program has been written which can operate the motors. As the other systems are finished, LabVIEW will be used to take over control of these systems. Future electronics could allow LabVIEW to monitor water flow, water temperature, filament current, background radiation levels and importantly, the x-ray detector signal. LabVIEW will be used to collect x-ray signal data, which can be graphed versus the position of the motors on the half-circle. This data can be then used with Bragg's Law to give the crystal structure.

*References*


[1] N. Robotti, Rendiconti Lincei **24,** S7-S18 (2013).
[2] Per F. Dahl, *Flash of the Cathode Rays: A history of JJ Thomson's Electron* (Institute of Physics Pub., Philadelphia, 1997).
[3] W. R. Hendee, Physics Today **48**, 51 (1995).
[4] C. Hammond, *The Basics of Crystallography and Diffraction: Third Edition* (Oxford University Press, New York, 2009).
[5] M. Eckert, Acta Crystallographica: Section A **68**, 30-39 (2012).
[6] J. D. Watson and F. H. C. Crick, Nature **171**, 737-738 (1953).
[7] W. H. and W. L. Bragg, *X rays and crystal structure* (G. Bell and sons, London, 1915).
[8] P. P. Ewald, *Fifty years of X-ray diffraction* (A. Oosthoek's Uitgeversmij, Utrecht, 1962).
[9] W. L. Bragg, Proceedings of the Royal Society of London. Series A, Containing Papers of a Mathematical and Physical Character **89**, 248-277 (1913).
[10] H. P. Rooksby, J. Sci. Intsrum. **18**, 84-90 (1941).
[11] W. A. Wood, Proc. Phys. Soc. **44**, 67-75 (1932).
[12] N. Kato, Acta Metallurgica **6**, 647-652 (1958).
[13] W. A. Wood, Trans. Faraday Soc. **31**, 1248-1263 (1935).
[14] A. Authier, *Dynamical theory of x-ray diffraction* (Oxford University Press, Oxford, 2001).
[15] J. O. McCaldin, J. Appl. Phys. **31**, 89 (1960).
[16] C. C. Wang and L. H. Spinar, Journal of Physics and Chemistry of Solids **24**, 953-955 (1963).
[17] S. P. Baker, B. Hoffman, L. Timian, A. Silvernail, E. A. Ellis (unpublished).
[18] J. Koike, M. Wada, M. Sanada, and K. Maruyama, Applied Physics Letters **81**, 1017-1019 (2002).
[19] E. E. Koch, *Handbook on synchrotron radiation*, (North Holland Pub. Co., New York, 1983).
[20] E. M. McMillan, Physical Review **68**, 143-144 (1945).
[21] V. Veksler, Phys. Rev. **69**, 244 (1946).
[22] C. V. Thompson and R. Carel, J. Mech. Phys. Solids, **44**, 657-673 (1996).
[23] C. Polop, C. Rosiepen, S. Bleikamp, R. Drese, J. Mayer, A. Dimyati, and T. Michely, New Journal of Physics **9**, 74 (2007).
[24] J. A. Floro, C. V. Thompson, R. Carel, and P.D. Bristowe, Journal of Materials Research **9**, 2411-2424 (1994).
[25] E. M. Zielinski, R. P. Vinci, and J. C. Bravman, Journal of Applied Physics **76**, 4516-4523 (1994).
[26] P. Sonnweber-Ribic, P. A. Gruber, G. Dehm, H. P. Strunk, and E. Arzt, Acta Materialia **60**, 2397-2406 (2012).
[27] J. Greiser, P. Müllner, and E. Arzt, Acta Materialia **49**, 1041-1050 (2001).
[28] H. Klug and L. Alexander, *X-ray Diffraction Procedures*, (John Wiley & Sons, New York, 1954).
[29] R. A. Serway and J. W. Jewett, Jr., *Physics for Scientists and Engineers, Seventh Edition*, (Thomson Higher Education, Belmont, 2008).